Multidimensional Upwind Fluctuation Distribution Schemes for Scalar Time Dependent Problems. *

M.E.Hubbard

The University of Reading, Department of Mathematics,

P.O.Box 220, Whiteknights, Reading, Berkshire, RG6 6AX, U.K.

and

P.L.Roe

Department of Aerospace Engineering,

University of Michigan, Ann Arbor, MI 48109-2118, U.S.A.

19th January 1998

*This work has been carried out as part of the Oxford/Reading Institute for Computational Fluid Dynamics and was funded by EPSRC.

Abstract

Some techniques for improving the accuracy of multidimensional upwind fluctuation distribution schemes for the scalar advection equation are compared. One involves the construction of a consistent Petrov-Galerkin finite element scheme which is equivalent to the fluctuation distribution scheme when mass-lumping is applied. Another uses a predictor-corrector technique to improve the approximation. In both cases monotonicity is imposed using a flux-corrected transport approach. A third method is then described which combines the second order accurate Lax-Wendroff scheme with the PSI scheme via a fluctuation redistribution step which ensures monotonicity (and which is a generalisation of the FCT approach for fluctuation distribution schemes). Furthermore, the concept of a distribution point is introduced, leading to a 'preferred direction' for the limiting procedure. Extensive numerical results are presented for each of these schemes.

1 Introduction

Over the last ten years a family of cell vertex finite volume methods for the solution of the two-dimensional scalar advection equation has evolved known as multidimensional upwind fluctuation distribution schemes [3]. For the approximation of steady state flows on unstructured triangular grids these have reached a degree of maturity whereby the multidimensional schemes reproduce most of the advantages of upwind schemes in one dimension: smooth, second order accurate solutions and rapid convergence to the steady state without the necessity for additional artificial viscosity.

Unfortunately, all of the current upwind distribution schemes are only first order accurate for time-dependent flows. Recently, this problem has been addressed with some success in [6] in which the schemes have been equated with upwind finite element algorithms, but only at the expense of inverting a full mass matrix. An alternative method, which takes the form of a predictor-corrector scheme, will be described for improving the accuracy of the approach for approximating unsteady solutions of the scalar advection equation. Both of these techniques lead to spurious oscillations in the solution close to steep gradients unless some form of limiting procedure is applied. Hence they are combined with a flux-corrected transport technique [5] to ensure monotonicity.

In this report a more sophisticated approach to enforcing monotonicity (of which flux-corrected transport is a special case) will be described which can be applied to any cell vertex fluctuation distribution scheme, such as the second order accurate Lax-Wendroff scheme [3]. The new method consists of a fluctuation *re*distribution step in which the distribution coefficients are altered to avoid the creation of new extrema by the nodal updates whilst retaining conservation.

The concept of a distribution point will be described and related to monotonicity conditions derived from the local solution. Furthermore, the equivalent equation will be used to construct a preferred direction for the movement of the distribution when the redistribution is applied. Extensive numerical results will then be presented to demonstrate the effectiveness of the new techniques.

In Section 2 the multidimensional upwind schemes currently used for solv-

ing steady state problems are described. This is followed in Sections 3 and 4 by descriptions of the consistent finite element method proposed in [6] and a predictor-corrector approach based on MacCormack's scheme. The next section describes the flux-corrected transport technique for imposing monotonicity on finite element and fluctuation distribution schemes while in Section 6 a new approach is suggested based on the notion of fluctuation redistribution. Results are presented for two time-dependent scalar advection test cases in Section 7 and some conclusions are drawn at the end.

2 A Steady State Scheme

Consider the two-dimensional scalar advection equation,

$$u_t + f_x + g_y \;=\; 0 \qquad \text{or} \qquad u_t + \vec{\lambda} \cdot \vec{\nabla} u \;=\; 0 \;, \tag{2.1}$$

where $\vec{\lambda} = \left(\frac{\partial f}{\partial u}, \frac{\partial g}{\partial u}\right)^{\mathrm{T}}$ defines the advection velocity. The fluctuation associated with this equation is the cell-based quantity given by

$$\begin{aligned} \phi \;&=\; -\int\!\!\int_{\triangle} \vec{\lambda} \cdot \vec{\nabla} u \; \mathrm{d}x \, \mathrm{d}y \\ &=\; \oint_{\partial \triangle} u \, \vec{\lambda} \cdot \mathrm{d}\vec{n} \;, \end{aligned} \tag{2.2}$$

where $\vec{n}$ represents the inward pointing normal to the boundary of the cell. In many cases ϕ can be evaluated exactly under an appropriate (conservative) linearisation of the equation (2.1) [3], in which case it can be written

$$\phi \;=\; -S_{\triangle} \widehat{\vec{\lambda}} \cdot \widehat{\vec{\nabla} u} \;, \tag{2.3}$$

where $S_{\triangle}$ is the cell area and the symbol $\widehat{\cdot}$ indicates an appropriately linearised quantity. For linear advection $\vec{\lambda}$ is constant so a conservative linearisation can be constructed simply by assuming that u varies linearly over each triangle with the discrete solution values stored at the nodes and continuity across the edges [3].

The numerical scheme is constructed from a discretisation of the integrated form of (2.1) by evaluating the quantity ϕ of (2.3) within each cell and then distributing it to the nodes of the grid. Combining this technique with a simple forward Euler discretisation of the time derivative leads to an iterative update of

the nodal solution values which can be written

$$u_i^{n+1} \;=\; u_i^n + \frac{\Delta t}{S_i} \sum_{\cup \triangle_i} \alpha_i^j \phi_j \;, \tag{2.4}$$

where S_i is the area of the median dual cell for node i (one third of the total area of the triangles with a vertex at i), α_i^j is the distribution coefficient which indicates the appropriate proportion of the fluctuation ϕ_j to be sent from cell j to node i, and $\cup \triangle_i$ represents the set of cells with vertices at node i.

2.1 The PSI Scheme

The distribution coefficients α_i^j are chosen so that the resulting scheme is conservative, linearity preserving (second order accurate at the steady state) and positive (monotonic). The word monotonic is slightly ambiguous when used in a two-dimensional context but will be used from now on to denote a scheme which doesn't create spurious extrema at the new time level.

The PSI scheme [3] has all of the above properties and is defined as follows:

1) For each triangle locate the downstream vertices, *i.e.* those for which

$$\hat{\vec{\lambda}} \cdot \vec{n}_i \;>\; 0 \;, \tag{2.5}$$

where $\vec{n}_i$ is the inward pointing normal to the edge opposite vertex i.

2a) If a triangle has a single downstream vertex, node i say, then that node receives the whole fluctuation, so

$$u_i \;\rightarrow\; u_i + \frac{\Delta t}{S_i} \phi \;, \tag{2.6}$$

while the values of u at the other two vertices remain unchanged.

2b) Otherwise, the triangle has two downstream vertices, i and j say, and the fluctuation is divided between these two nodes so that

$$\begin{aligned} u_i \;&\rightarrow\; u_i + \frac{\Delta t}{S_i} \phi_i^* \;, \\ u_j \;&\rightarrow\; u_j + \frac{\Delta t}{S_j} \phi_j^* \;, \end{aligned} \tag{2.7}$$

where $\phi_i^* + \phi_j^* = \phi$.

The fluctuations in (2.7) are defined as the limited quantities,

$$\begin{aligned} \phi_i^* &= \phi_i - L(\phi_i, -\phi_j) \ , \\ \phi_j^* &= \phi_j - L(\phi_j, -\phi_i) \ , \end{aligned} \tag{2.8}$$

where

$$\phi_i \ = \ -\frac{1}{2}\widehat{\vec{\lambda}} \cdot \vec{n}_i (u_i - u_k) \ , \quad \phi_j \ = \ -\frac{1}{2}\widehat{\vec{\lambda}} \cdot \vec{n}_j (u_j - u_k) \ , \tag{2.9}$$

in which k denotes the remaining (upstream) vertex of the triangle and L denotes the minmod limiter function,

$$L(x,y) \ = \ \frac{1}{2}(1 + \mathrm{sgn}(xy)) \frac{1}{2}(\mathrm{sgn}(x) + \mathrm{sgn}(y)) \min(|x|, |y|) \ . \tag{2.10}$$

The scheme is globally positive and therefore stable, the appropriate restriction on the time-step being

$$\Delta t \ \leq \ \frac{S_i}{\sum_{j \in \cup \triangle_i} \max\left(0, \frac{1}{2}\widehat{\vec{\lambda}^j} \cdot \vec{n}_i^j\right)} \ . \tag{2.11}$$

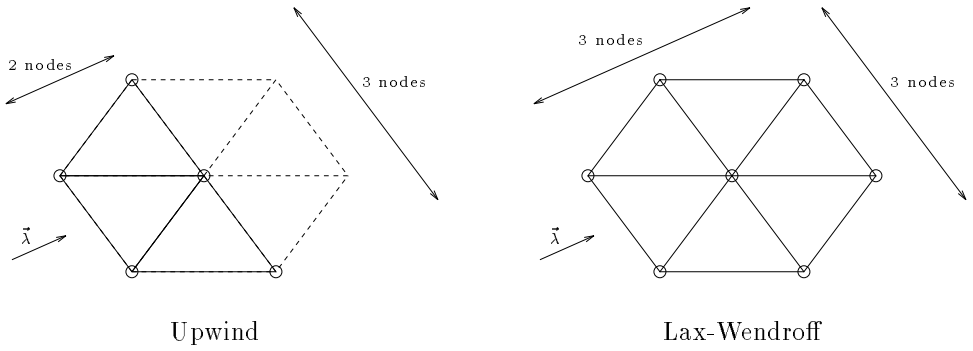

Figure 2.1: The stencils of the PSI scheme and the Lax-Wendroff scheme.

The above algorithm is second order accurate only at the steady state. This is not surprising since the limiter in step b) above is taking the contributions ϕ_i and ϕ_j (2.9) due to the first order N scheme [3] and redistributing the fluctuation between the two downstream vertices (along the outflow edge) which, in some sense, is giving second order accuracy in the cross-stream direction. The scheme is only first order accurate in the streamwise direction (in fact on a regular grid with edges aligned with the flow it reduces to the one-dimensional first order upwind scheme) but at the steady state this is irrelevant because the solution

is constant parallel to the streamlines. This is illustrated further in Figure 2.1 which shows the stencil of the upwind scheme and this has only two nodes in the streamwise direction but three for crossflow.

In the following sections the PSI scheme will be modified to improve its accuracy for approximating time varying solutions of the two-dimensional scalar advection equation on triangular grids.

2.2 The Lax-Wendroff Distribution Scheme

The Lax-Wendroff scheme [3] does not have the restricted stencil of the PSI scheme and this allows it to attain second order accuracy. In fact it is the unique single step second order accurate fluctuation distribution scheme on triangles with a compact stencil (as in Figure 2.1). The distribution coefficients in (2.4) which lead to this scheme are

$$\alpha_i^j \;=\; \frac{1}{3} + \frac{\Delta t}{4S_{\triangle_j}} \vec{\lambda} \cdot \vec{n}_i^j \;, \tag{2.12}$$

where $S_{\triangle_j}$ is the area of the j^{th} cell and $\vec{n}_i^j$ is the scaled inward pointing normal to the edge of triangle j opposite the vertex at node i. The limit on the time-step at a node i for the stability of this scheme is taken to be

$$\Delta t \;\leq\; 2 \min_{j \in \cup_{\triangle_i}} \left(\frac{S_{\triangle_j}}{\max_{l=1,2,3} \left(|\vec{\lambda} \cdot \vec{n}_l^j| \right)} \right) \;, \tag{2.13}$$

where l covers the vertices of each cell in the local patch surrounding the node.

2.3 Area weighting of Nodal Updates

The accuracy of low order fluctuation distribution schemes (such as PSI) can be improved slightly by altering the weighting of the nodal updates in a manner which ensures that linear initial data on an arbitrary grid remains linear after each time-step [1].

Given linear data, $(\vec{\lambda} \cdot \vec{\nabla} u)$ is constant throughout the domain so the general nodal update (2.4) takes the form

$$u_i^{n+1} \;=\; u_i^n + \frac{\Delta t}{S_i} \sum_{\cup \triangle_i} \alpha_i^j S_{\triangle_j} \, K \;, \tag{2.14}$$

where $K = -\vec{\lambda} \cdot \vec{\nabla} u$. Therefore, replacing S_i in (2.14) by $\sum_{\cup \triangle_i} \alpha_i^j S_{\triangle_j}$ gives the same increment at each node and hence the data remains linear at the new time level. The resulting nodal update is

$$u_i^{n+1} \;=\; u_i^n + \frac{\Delta t}{\sum_{\cup \triangle_i} \alpha_i^j S_{\triangle_j}} \sum_{\cup \triangle_i} \alpha_i^j \phi_j \;. \tag{2.15}$$

Note that this modification has no effect on the conservative nature of the distribution scheme. In fact, on regular grids in which six triangles surround each interior node the two schemes (2.4) and (2.14) are the same. It can also be shown that the area weighting of (2.14) leaves the Lax-Wendroff scheme unaltered.

3 The Finite Element Approach

Any fluctuation distribution scheme, such as the PSI scheme described above, can be equated with a mass-lumped Petrov-Galerkin finite element scheme, and in one dimension it is well known that using a consistent finite element formulation generally leads to a significant increase in spatial accuracy over the corresponding mass-lumped scheme. For example, applying a consistent mass matrix to the first order upwind scheme increases its spatial accuracy to third order in one dimension [6], so a similar improvement might be hoped for in the two-dimensional case.

In the previous section it was assumed that the approximate solution u was continuous and varied linearly over each triangle with the discrete values being stored at the nodes. In finite element terms this means that the solution can be written

$$u(x,y,t) \;=\; \sum_{i=1}^{N_n} u_i(t)\, \omega_i(x,y) \;, \tag{3.1}$$

where N_n is the number of grid nodes and $\omega_i(x,y)$ are the standard linear trial functions. It remains to choose the test functions so that the mass-lumped scheme is equivalent to the chosen fluctuation distribution scheme.

In [6] an SUPG-type test function is adopted. This takes the form

$$\psi_i \;=\; \omega_i + \sum_{\cup \triangle_i} \beta_i^j \kappa_j \;, \tag{3.2}$$

where κ_j takes a value of 1 on cell j and zero elsewhere, and β_i^j are coefficients corresponding to the contribution of cell j to node i and are yet to be determined.

Forcing the equivalence of the mass-lumped Petrov-Galerkin scheme to the fluctuation distribution scheme (2.4) requires that the test functions ψ_i should be chosen to satisfy

$$-\int\int_{\triangle_j} \psi_i \, \vec{\lambda} \cdot \vec{\nabla} u \, \mathrm{d}x \, \mathrm{d}y \;=\; \alpha_i^j \phi_j \;, \tag{3.3}$$

where α_i^j are the distribution coefficients of (2.4). Combining this with the fact that the fluctuation is given by

$$\phi_j \;=\; -\int\int_{\triangle_j} \vec{\lambda} \cdot \vec{\nabla} u \, \mathrm{d}x \, \mathrm{d}y \;, \tag{3.4}$$

implies that the coefficients in (3.2) are defined by

$$\beta_i^j \;=\; \alpha_i^j - \frac{1}{\phi_j} \int\int_{\triangle_j} \omega_i \, \vec{\lambda} \cdot \vec{\nabla} u \, \mathrm{d}x \, \mathrm{d}y \;. \tag{3.5}$$

From (3.3) and (3.5) it can be seen that a pure Galerkin finite element discretisation with linear test and trial functions ($\psi_i = \omega_i$) leads straightforwardly to $\beta_i^j = 0$ and a distribution coefficient for the equivalent finite volume scheme of the form

$$(\alpha_i^j)_{\mathrm{G}} \;=\; \frac{1}{\phi_j} \int\int_{\triangle_j} \omega_i \, \vec{\lambda} \cdot \vec{\nabla} u \, \mathrm{d}x \, \mathrm{d}y \;. \tag{3.6}$$

Thus, (3.5) implies that the general form of the test functions is given by

$$\psi_i \;=\; \omega_i + \sum_{\cup \triangle_i} (\alpha_i^j - (\alpha_i^j)_{\mathrm{G}}) \, \kappa_j \;, \tag{3.7}$$

where the α_i^j are the distribution coefficients pertaining to the chosen fluctuation distribution scheme [3].

The use of piecewise linear trial and test functions means that the finite element integrals are easy to evaluate. In particular (3.6) becomes

$$(\alpha_i^j)_{\mathrm{G}} \;=\; \frac{1}{3} \;, \tag{3.8}$$

and consequently

$$\psi_i \;=\; \omega_i + \sum_{\cup \triangle_i} \left(\alpha_i^j - \frac{1}{3} \right) \kappa_j \;. \tag{3.9}$$

The consistent mass matrix for this scheme can now be assembled from the individual element contributions which take the form

$$\mathbf{M}_k \;=\; \{m_{i,j}\}_k \;=\; \int\int_{\triangle_k} \psi_i \, \omega_j \, \mathrm{d}x \, \mathrm{d}y \;, \tag{3.10}$$

in which i and j represent global node indices and k is the cell index. The nonzero components are easily calculated to be

$$\mathbf{M}_k \;=\; \frac{S_{\triangle_k}}{3}\begin{pmatrix} \frac{1}{2}+\alpha_1^k-\frac{1}{3} & \frac{1}{4}+\alpha_1^k-\frac{1}{3} & \frac{1}{4}+\alpha_1^k-\frac{1}{3} \\ \frac{1}{4}+\alpha_2^k-\frac{1}{3} & \frac{1}{2}+\alpha_2^k-\frac{1}{3} & \frac{1}{4}+\alpha_2^k-\frac{1}{3} \\ \frac{1}{4}+\alpha_3^k-\frac{1}{3} & \frac{1}{4}+\alpha_3^k-\frac{1}{3} & \frac{1}{2}+\alpha_3^k-\frac{1}{3} \end{pmatrix} , \tag{3.11}$$

where α_i^k is the distribution coefficient associated with the i^{th} vertex of the k^{th} cell, so the assembled mass matrix is given by

$$\mathbf{M} \;=\; \{m_{i,j}\} \;=\; \sum_{k=1}^{N_c} \mathbf{M}_k \;, \tag{3.12}$$

where N_c is the number of grid cells. The scheme therefore takes the form

$$\sum_{j=1}^{N_n} m_{i,j}\frac{\mathrm{d}u_j}{\mathrm{d}t} \;=\; -\sum_{\cup\triangle_i} \alpha_i^k \phi_k \quad \text{for} \quad i = 1, ..., N_n \;, \tag{3.13}$$

where N_n is the number of grid nodes.

The mass matrix $\mathbf{M}$ is not symmetric so in the experiments which follow its inversion is carried out using the GMRES(40) algorithm, which is described in detail in [10, 11]. The right hand side of (3.13) is precisely that of the fluctuation distribution approach and mass-lumping leads to a scheme of the form

$$S_i\frac{\mathrm{d}u_i}{\mathrm{d}t} \;=\; -\sum_{\cup\triangle_i} \alpha_i^k \phi_k \quad \text{for} \quad i = 1, ..., N_n \;, \tag{3.14}$$

so combining this with a forward Euler time discretisation is equivalent to (2.4).

3.1 High Order Time-Accuracy

Second order accuracy in time is achieved using the implicit discretisation [4]

$$\left(\frac{\mathbf{M}}{\Delta t} - \theta\mathbf{J}\right)(\underline{U}^{n+1} - \underline{U}^n) \;=\; \underline{R}^n \;, \tag{3.15}$$

in which $\mathbf{M}$ is the assembled mass matrix, $\underline{U}$ is the vector of nodal variables and $\underline{R}$ is the vector of nodal residuals (*i.e.* the right hand side of (3.13)). $\mathbf{J} = \frac{\partial \underline{R}}{\partial \underline{U}}$ is the linearised Jacobian and may be evaluated numerically using

$$\frac{\partial R_i(\underline{U}^n)}{\partial U_j^n} \;\approx\; \frac{R_i(\underline{U}^n + \epsilon\underline{1}_j) - R_i(\underline{U}^n)}{\epsilon} \;, \tag{3.16}$$

where $\underline{1}_j$ is the vector of zeros with 1 in the j^{th} entry and ϵ is a small parameter (taken here to be 10^{-10}).

When $\theta = 0$ in (3.15) the temporal discretisation is first order (forward Euler). Second order accuracy is achieved by choosing $\theta = \frac{1}{2}$ which gives a Crank-Nicolson algorithm. Note that the matrix $\left(\frac{\mathbf{M}}{\Delta t} - \theta \mathbf{J}\right)$ in (3.15) is generally no more expensive to invert than the mass matrix on its own, so implicit time-stepping can be used to allow larger time-steps to be taken with a negligible increase in the cost. In practice though, it has proved to be difficult to significantly increase the time-step without a dramatic loss of accuracy in the solution.

4 A Predictor-Corrector Approach

A second technique which has been widely used in one dimension to create schemes with high order accuracy is the predictor-corrector approach. This has the advantage over the consistent finite element scheme in that no matrix inversion is necessary.

The predictor-corrector approach is demonstrated simply in one dimension by MacCormack's scheme [7] for the scalar advection equation,

$$u_t + f_x \;=\; 0 \;. \tag{4.1}$$

The first (predictor) step of the algorithm calculates and stores the update due to the standard first order upwind scheme, which for $\frac{\partial f}{\partial u} > 0$ is given by

$$\begin{aligned} \overline{u_i} &= u_i^n - \frac{\Delta t}{\Delta x}(f_i^n - f_{i-1}^n) \\ &= u_i^n + \frac{\Delta t}{\Delta x}\phi_{i-1/2} \;, \end{aligned} \tag{4.2}$$

where ϕ represents the one-dimensional fluctuation.

The corrector step is applied to cancel out the leading order error terms in the first order approximation of the predictor step. One way to achieve this is to take a backward space difference given by

$$\begin{aligned} \overline{\overline{u_i}} &= u_i - \frac{\Delta t}{\Delta x}(\overline{f_{i+1}} - \overline{f_i}) \\ &= u_i - \frac{\Delta t}{\Delta x}\overline{\phi_{i+1/2}} \;, \end{aligned} \tag{4.3}$$

where $\overline{f} = f(\overline{u})$, and then to average the two updates, so that the final scheme takes the form

$$\begin{aligned} u_i^{n+1} &= \frac{1}{2}(\overline{u_i} + \overline{\overline{u_i}}) \\ &= u_i^n - \frac{\Delta t}{2\Delta x}((f_i^n - f_{i-1}^n) + (\overline{f_{i+1}} - \overline{f_i})) \\ &= u_i^n - \frac{\Delta t}{2\Delta x}(\phi_{i-1/2} + \overline{\phi_{i+1/2}}) \ . \end{aligned} \tag{4.4}$$

In the case of linear advection, $f = \lambda u$ where λ is a constant and so on a uniform grid one can define $\nu = \frac{\lambda \Delta t}{\Delta x}$ so that (4.4) becomes

$$\begin{aligned} u_i^{n+1} &= u_i^n - \frac{1}{2}\nu(1-\nu)(u_{i+1}^n - u_i^n) - \frac{1}{2}\nu(1+\nu)(u_i^n - u_{i-1}^n) \\ &= u_i^n + \frac{\Delta t}{\Delta x}\left(\frac{1}{2}(1-\nu)\phi_{i+1/2} + \frac{1}{2}(1+\nu)\phi_{i-1/2}\right) \ , \end{aligned} \tag{4.5}$$

which is precisely the Lax-Wendroff scheme written in finite difference and fluctuation distribution form respectively.

Equivalently, the corrector stage (4.3) can be constructed from a reversal of both the temporal and spatial discretisations such that

$$\overline{\overline{u_i}} \ = \ \overline{u_i} + \frac{\Delta t}{\Delta x}(\overline{f_{i+1}} - \overline{f_i}) \ , \tag{4.6}$$

which is very similar to (4.3) and is equivalent to upwinding backwards in time. This approximation provides a correction to the predicted update which leads to a scheme of the form

$$u_i^{n+1} \ = \ \overline{u_i} + \frac{1}{2}(u_i^n - \overline{\overline{u_i}}) \ , \tag{4.7}$$

cf. (4.4). As before this reduces to the Lax-Wendroff scheme (4.5) for linear advection on a uniform grid.

Now consider the multidimensional case. The predictor step can be any (preferably monotonic) fluctuation distribution scheme,

$$S_i(\overline{u_i} - u_i^n) \ = \ \Delta t \sum_{\cup \Delta_i} \alpha_i^j \phi_j \ , \tag{4.8}$$

so here it is chosen to be the PSI scheme described in Section 2. The corresponding backward space difference is easily obtained by reversing the sign of $\hat{\vec{\lambda}}$ in the calculation of the distribution coefficients $\overline{\alpha_i^j}$ so that

$$S_i(\overline{\overline{u_i}} - u_i^n) \ = \ \Delta t \sum_{\cup \Delta_i} \overline{\alpha_i^j}\,\overline{\phi_j} \ , \tag{4.9}$$

and taking the average of the two updates gives

$$\begin{aligned} u_i^{n+1} &= \frac{1}{2}(\overline{u_i} + \overline{\overline{u_i}}) \\ &= u_i^n + \frac{\Delta t}{2S_i} \sum_{\cup \triangle_i} \left(\alpha_i^j \phi_j + \overline{\alpha_i^j} \overline{\phi_j} \right) \ . \end{aligned} \tag{4.10}$$

If the corrector step is thought of in terms of reversing the temporal discretisation then the second stage becomes

$$S_i(\overline{u_i} - \overline{\overline{u_i}}) \ = \ \Delta t \sum_{\cup \triangle_i} \overline{\alpha_i^j} \overline{\phi_j} \ , \tag{4.11}$$

and, as in one dimension, it leads to an equivalent update of

$$u_i^{n+1} \ = \ \overline{u_i} + \frac{1}{2}(u_i^n - \overline{\overline{u_i}}) \ . \tag{4.12}$$

The similarity of the predictor-corrector scheme to the two-dimensional Lax-Wendroff scheme can be illustrated by considering some simple examples of linear advection on regular grids such as those shown in Figure 4.1.

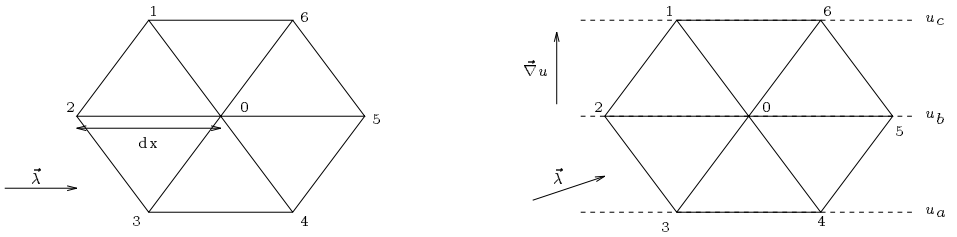

Figure 4.1: Examples of the equivalence of the predictor-corrector method with a Lax-Wendroff scheme.

In the first case the data is arbitrary but the advection velocity is aligned with one set of grid edges. Simple analysis shows that the predictor-corrector update for the central node is given by

$$u_i^{n+1} \ = \ u_i^n - \frac{1}{2}\nu(1-\nu)(u_5^n - u_0^n) - \frac{1}{2}\nu(1+\nu)(u_0^n - u_2^n) \ , \tag{4.13}$$

which is simply a one-dimensional Lax-Wendroff scheme where

$$\nu \ = \ \frac{\vec{\lambda} \cdot (\vec{n}_{12} + \vec{n}_{23}) \Delta t}{2S_0} \ = \ \frac{|\vec{\lambda}| \Delta t}{dx} \ , \tag{4.14}$$

in which dx is the distance between nodes 2 and 0 and S_0 is the area associated with the central node.

The second example shown in Figure 4.1 uses data whose gradient is perpendicular to one set of grid edges but the advection velocity is now arbitrary. The predictor-corrector scheme again reduces to a Lax-Wendroff style update, this time taking the form

$$u_i^{n+1} \;=\; u_i^n - \frac{1}{2}\nu(1-\nu)(u_c^n - u_b^n) - \frac{1}{2}\nu(1+\nu)(u_b^n - u_a^n)\;, \tag{4.15}$$

where now

$$\nu \;=\; \frac{\vec{\lambda}\cdot\vec{n}_{20}\Delta t}{S_0} \;=\; \frac{|\vec{\lambda}|\cos\theta\Delta t}{dx}\;, \tag{4.16}$$

and θ is the angle between $\vec{\lambda}$ and $\vec{\nabla}u$. In this case the two-dimensional Lax-Wendroff scheme of (2.12), also reduces to (4.15) while each of the fully upwind schemes leads to a form of first order upwinding, *i.e.*

$$u_i^{n+1} \;=\; u_i^n - \nu(u_b^n - u_a^n)\;, \tag{4.17}$$

in which ν is as in (4.16).

4.1 A Single Step Scheme

The above formulation does not result in a single step fluctuation distribution scheme as it did in one dimension (4.5) but it does provide hints as to how such a goal might be achieved. For example, distribution coefficients may be evaluated as follows:

- Calculate the distribution coefficients α_i^j for the chosen fluctuation distribution scheme, say the PSI scheme.
- Reverse the direction of the flow (but not the sign of the fluctuation) and calculate a second set of distribution coefficients $\overline{\alpha_i^j}$.
- Apply a Lax-Wendroff style redistribution along the two edges which join the upstream node(s) to the downstream node(s), so if two vertices (2 and 3 say) are initially downstream then

$$\begin{aligned}
\alpha_1^j &\;\rightarrow\; \frac{1}{2}(1-\nu_2)\alpha_2^j + \frac{1}{2}(1-\nu_3)\alpha_3^j \\
\alpha_2^j &\;\rightarrow\; \frac{1}{2}(1+\nu_2)\alpha_2^j \\
\alpha_3^j &\;\rightarrow\; \frac{1}{2}(1+\nu_3)\alpha_3^j\;,
\end{aligned} \tag{4.18}$$

whereas if only one vertex is downstream (vertex 1) then

$$\begin{aligned}
\alpha_1^j &\rightarrow \frac{1}{2}(1+\nu_2)\overline{\alpha_2^j} + \frac{1}{2}(1+\nu_3)\overline{\alpha_3^j} \\
\alpha_2^j &\rightarrow \frac{1}{2}(1-\nu_2)\overline{\alpha_2^j} \\
\alpha_3^j &\rightarrow \frac{1}{2}(1-\nu_3)\overline{\alpha_3^j} \ , \qquad (4.19)
\end{aligned}$$

where $\nu_i = \frac{\widehat{\vec{\lambda}}.\vec{l}_i \, \Delta t}{S_\Delta}$ and $\vec{l}_i$ is the edge opposite vertex i taken in the downstream direction.

This scheme is still conservative since it remains true that

$$\alpha_1^j + \alpha_2^j + \alpha_3^j \ = \ 1 \quad \forall \, j \ , \qquad (4.20)$$

and it reduces to the predictor-corrector scheme (and hence Lax-Wendroff) when the flow is parallel to the edges of a regular grid. Its major advantage over the two stage scheme is that of speed. However, in practice the scheme described above lacks robustness and is far less reliable than the Lax-Wendroff scheme.

5 Flux-Corrected Transport Techniques

As it stands, none of the above higher order algorithms is monotonic so spurious oscillations can appear in the numerical solutions. In the case of the predictor-corrector and Lax-Wendroff schemes these are, as expected, usually to be found immediately upstream of steep flow gradients.

A simple and widely used approach to the imposition of monotonicity on a scheme is the flux-corrected transport (FCT) technique [5, 12] which will be described here in the context of fluctuation distribution schemes. In the next section a more sophisticated approach will be described which can be applied to the single step Lax-Wendroff distribution scheme.

Flux-corrected transport requires a combination of two numerical schemes, a low order monotonic scheme, taken here to be the PSI scheme of Section 2, and a high order (non-monotonic) scheme to which the smoothing is to be applied, such as those described in Sections 3 and 4. In the finite element and fluctuation distribution contexts FCT requires that each scheme be written in a form which

isolates the contribution from each individual grid cell to the nodes of the grid. An antidiffusive cell contribution is then calculated by taking the difference between the high order and low order contributions, and this is limited in such a way as to prohibit unwanted extrema in the solution whilst retaining as much of the antidiffusive component as possible. As a result, the high order scheme should dominate the algorithm in smooth regions of the flow while the scheme may well return to first order in regions where the solution gradient is high.

The FCT algorithm is described by the following six steps:

1. Compute the Low order Element Contributions (LEC) from the mass-lumped PSI scheme.

2. Compute the High order Element Contributions (HEC) from the consistent PSI scheme, the predictor-corrector scheme or the Lax-Wendroff scheme.

3. Calculate the Antidiffusive Element Contributions (AEC) given by

$$\text{AEC} \;=\; \text{HEC} - \text{LEC}\;. \tag{5.1}$$

4. Compute the updated low order solution,

$$u_i^{\text{L}} \;=\; u_i^n + \sum_{\cup \triangle_i} \text{LEC} \qquad \forall\, i\;. \tag{5.2}$$

5. Correct the AEC in a manner such that the new solution (as defined in step 6) has no extrema not also found in either u_i^{L} or u_i^n, so

$$\text{AEC}^c \;=\; C_T \times \text{AEC} \quad \text{where} \quad 0 \le C_T \le 1\;. \tag{5.3}$$

6. Calculate the final solution update,

$$u_i^{n+1} \;=\; u_i^L + \sum_{\cup \triangle_i} \text{AEC}^c\;. \tag{5.4}$$

The limiting procedure of step 5 is designed to make AEC^c as large as possible without introducing new extrema or knowing in advance the nodal updates due to the high order scheme in adjacent cells. It involves the following calculations:

- Evaluate in order the quantities

$$\begin{aligned} u_i^* &= \begin{cases}\max \\ \min\end{cases} (u_i^{\mathrm{L}}, u_i^n) \\ u_T^* &= \begin{cases}\max \\ \min\end{cases} (u_1^*, u_2^*, u_3^*) \\ u_i^{\substack{\max \\ \min}} &= \begin{cases}\max \\ \min\end{cases} u_T^* \qquad \forall\, T \in \cup\triangle_i\ , \end{aligned} \tag{5.5}$$

  the last of which give the extreme values of the solution at each node i beyond which the updated solution is not allowed to go.

- Define

$$\begin{aligned} P_i^{\pm} &= \sum_{\cup\triangle_i} \begin{matrix}\max \\ \min\end{matrix} (0, \mathrm{AEC}) \\ Q_i^{\pm} &= u_i^{\substack{\max \\ \min}} - u_i^{\mathrm{L}} \end{aligned} \tag{5.6}$$

  and subsequently

$$R_i^{\pm} = \begin{cases} \min\left(1, Q_i^{\pm}/P_i^{\pm}\right) & \text{if } P_i^+ > 0,\ P_i^- < 0 \\ 0 & \text{if } P_i^{\pm} = 0\ , \end{cases} \tag{5.7}$$

  a nodal limiting factor for the antidiffusive contribution which ensures that the new solution value at node i does not violate the prescribed bounds.

- Finally calculate each element's limiting factor from the nodal values at its vertices so that

$$C_T = \min_{\text{vertices}} \begin{cases} R_i^+ & \text{if AEC} > 0 \\ R_i^- & \text{if AEC} < 0\ . \end{cases} \tag{5.8}$$

The above limiting is applied to the difference between the *element* contributions of the two underlying schemes.

In the case of the low order PSI scheme the splitting into element contributions is simple since the vector of nodal residuals $\underline{R}^n$ is assembled from the aforementioned element contributions and it is clear from (3.14) that a single component takes the form

$$R_i = \sum_{\cup\triangle_i} \alpha_i^k \phi_k = \sum_{\cup\triangle_i} R_i^k\ , \tag{5.9}$$

a simple sum of element contributions. Thus, the fact that

$$\mathbf{M}_L\, \Delta_n \underline{U}^{\mathrm{L}} = -\underline{R}^n\ , \tag{5.10}$$

in which $\mathbf{M}_L$ is the lumped mass matrix and the symbol $\Delta_n(\cdot) = (\cdot)^{n+1} - (\cdot)^n$ represents a time difference, implies that the element contribution from cell k to node i can be written

$$\mathrm{LEC}_i^k \;=\; \mathbf{M}_L{}^{-1}\,(\alpha_i^k\,\phi_k)\,\underline{1}_i\;, \tag{5.11}$$

in which $\underline{1}_i$ is the zero vector with i^{th} component 1. $\mathbf{M}_L$ is a diagonal matrix so that all of the inversion operations are local.

In the predictor-corrector case, precisely the same analysis applies to the high order scheme when it is derived from the average of a forward and a backward space differencing except that the definition of the residual has changed, *cf.* (4.10). The high order element contribution is defined by

$$\mathrm{HEC}_i^k \;=\; \frac{1}{2}\mathbf{M}_L{}^{-1}\left(\alpha_i^k\,\phi_k + \overline{\alpha_i^k}\,\overline{\phi_k}\right)\underline{1}_i\;, \tag{5.12}$$

so that the antidiffusive element contribution evaluated in step 3 of the FCT algorithm is straightforward to calculate and the limiting can then be applied.

The consistent finite element scheme cannot be treated in the same manner because although it is true that

$$\mathbf{M}_C\;\Delta_n\underline{U}^{\mathrm{H}} \;=\; -\underline{R}^n\;, \tag{5.13}$$

the consistent mass matrix $\mathbf{M}_C$ is not diagonal so inverting it results in each component of the residual (5.9) having a global effect on the nodal updates. Instead, it is noted that

$$\mathbf{M}_L\Delta_n\underline{U}^{\mathrm{H}} \;=\; \underline{R}^n + (\mathbf{M}_L - \mathbf{M}_C)\,\Delta_n\underline{U}^{\mathrm{H}}\;, \tag{5.14}$$

from which it immediately follows that the antidiffusive terms can be written as

$$\Delta_n\underline{U}^{\mathrm{H}} - \Delta_n\underline{U}^{\mathrm{L}} \;=\; \mathbf{M}_L{}^{-1}(\mathbf{M}_L - \mathbf{M}_C)\,\Delta_n\underline{U}^{\mathrm{H}}\;, \tag{5.15}$$

so the individual element contributions are given by

$$\mathrm{AEC}^k \;=\; \mathbf{M}_L{}^{-1}\,(\mathbf{M}_L - \mathbf{M}_C)_k\;\Delta_n\underline{U}^{\mathrm{H}}\;, \tag{5.16}$$

where the subscript k on the right hand side indicates the k^{th} element mass matrix as defined in (3.11). Now (5.16) defines the antidiffusive element contributions as local quantities so the limiting procedure described earlier can proceed.

FCT techniques are applied to the implicit time-stepping of (3.15) in precisely the same manner. The low order scheme is once more taken to be the explicit mass-lumped PSI scheme and the high order scheme is the implicit consistent PSI scheme. The above analysis is then repeated, replacing the consistent mass matrix by the corresponding matrix for the implicit scheme, *i.e.*

$$\mathbf{M}_C \;\rightarrow\; \mathbf{M}_C + \theta\Delta t\mathbf{J}\;. \tag{5.17}$$

The residual $\underline{R}$ from which the Jacobian $\mathbf{J} = \frac{\partial \underline{R}}{\partial \underline{U}}$ is calculated has already been written in terms of element contributions in (5.9) and it follows that the element components of $\mathbf{J}$ can be assembled from the derivatives

$$\mathbf{J}^k_{i,j} \;=\; \sum_{\cup\triangle_i} \frac{\partial R^k_i}{\partial U_j} \quad \text{for} \quad j = 1, ..., N_n\;. \tag{5.18}$$

Since each residual component R^k_i depends only on the solution values at the vertices of its own cell, denoted here by the superscript k, $\mathbf{J}$ reduces to an assembly of 3×3 components in the same manner as $\mathbf{M}_C$ and the new matrix of (5.17) can thus be treated in the same way during the FCT stage of the algorithm.

6 Limiting by Fluctuation Redistribution

FCT has proved to be an extremely successful technique for limiting fluxes to impose monotonicity but a loss of accuracy relative to the high order scheme, particularly noticeable when checking the error in the L_∞ norm, is unavoidable at turning points in the solution. In the fluctuation distribution framework a far more flexible technique for imposing accuracy is to redistribute the fluctuation as distributed initially by the high order scheme.

The Lax-Wendroff scheme, as given by (2.12), is a single step fluctuation distribution scheme and it is possible to combine it with the PSI scheme via redistribution to ensure monotonicity with a minimal loss of accuracy. The technique will be described below and FCT will be shown to be a special case of this new limiting technique.

6.1 The Distribution Point

A useful geometric interpretation of fluctuation distribution schemes is given by the concept of a distribution point. Consider a single grid cell in isolation: the distribution point is defined to be the point whose local area coordinates are the distribution coefficients for that triangle. Unless stated otherwise, it will be assumed from now on that the distribution coefficients are non-negative (true for both the Lax-Wendroff and PSI schemes) so that the distribution point is within the cell. Figure 6.1 shows typical distribution points for the two schemes which will be considered in this section. Note that the distribution point will lie on the outflow edge (or at the downstream vertex of a cell with one inflow edge) of the triangle when the scheme is fully upwind.

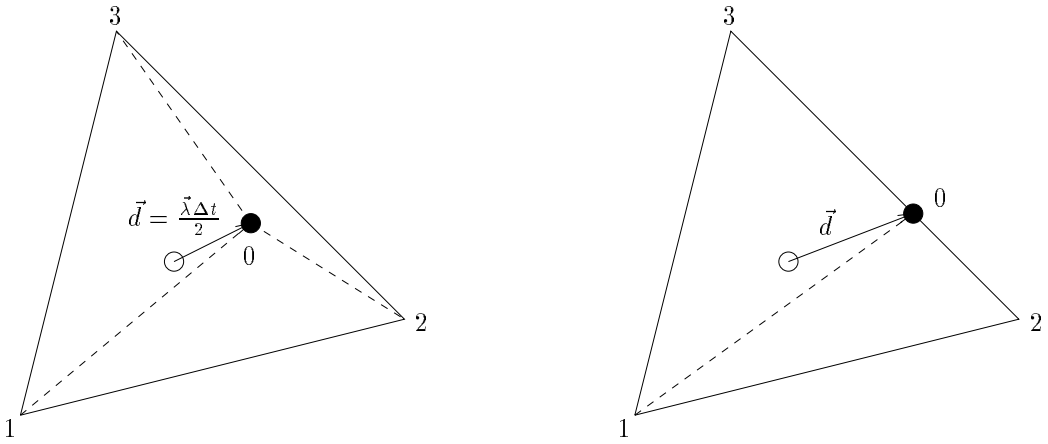

Figure 6.1: The position of the distribution point for the Lax-Wendroff scheme (left) and in the two-target case for a fully upwind scheme, *e.g.* PSI (right).

The relationship between the distribution coefficients and the local area coordinates can be written explicitly using the numbering of Figure 6.1 as

$$\alpha_1 \;=\; \frac{\text{Area}\,230}{\text{Area}\,123}\,, \quad \alpha_2 \;=\; \frac{\text{Area}\,310}{\text{Area}\,123}\,, \quad \alpha_3 \;=\; \frac{\text{Area}\,120}{\text{Area}\,123}\,, \tag{6.1}$$

from which it is obvious from this that

$$\alpha_1 + \alpha_2 + \alpha_3 \;=\; 1\,, \tag{6.2}$$

so the scheme is conservative, and that $\alpha_k \geq 0$ as long as the distribution point remains within the triangle.

It is useful to note that the movement of the distribution point is equivalent to the *re*distribution of the fluctuation within the triangle. Furthermore, moving the distribution point parallel to an edge is equivalent to keeping the proportion of the fluctuation being sent to the opposite vertex constant, *i.e.* the redistribution is taking place between the two nodes on that edge.

6.2 The Equivalent Equation

The diffusion vector $\vec{d}$ labelled in Figure 6.1 represents the displacement of the distribution point from the centroid of the triangle (the distribution point of a symmetric central scheme). It can easily be shown by geometric arguments that the distribution coefficients of any scheme defined locally by the diffusion vector $\vec{d}$ are given by

$$\alpha_i^j \;=\; \frac{1}{3} + \frac{1}{2S_{\triangle_j}} \vec{d} \cdot \vec{n}_i^j \;. \tag{6.3}$$

The relationship with the Lax-Wendroff scheme is obvious and comparison with (2.12) immediately gives

$$\vec{d} \;=\; \frac{\vec{\lambda}\Delta t}{2} \tag{6.4}$$

in this case, as noted in Figure 6.1.

Further, a scheme with diffusion vector $\vec{d}$ can be shown [9] to have the second order equivalent equation

$$u_t + \vec{\lambda} \cdot \vec{\nabla} u \;=\; \vec{d} \cdot \vec{\nabla}(\vec{\lambda} \cdot \vec{\nabla} u) \;, \tag{6.5}$$

in which the right hand side represents the numerical diffusion of the distribution scheme and can be used to analyse the accuracy of the method.

The diffusion vector of the Lax-Wendroff scheme (6.4) can be introduced into the equivalent equation by rewriting (6.5) as

$$u_t + \vec{\lambda} \cdot \vec{\nabla} u \;=\; \frac{\vec{\lambda}\Delta t}{2} \cdot \vec{\nabla}(\vec{\lambda} \cdot \vec{\nabla} u) + \left(\vec{d} - \frac{\vec{\lambda}\Delta t}{2} \right) \cdot \vec{\nabla}(\vec{\lambda} \cdot \vec{\nabla} u) \;. \tag{6.6}$$

The first term on the right hand side of (6.6) represents the numerical diffusion of the Lax-Wendroff scheme, which is second order accurate, while the second term provides additional dissipation which decreases the accuracy of the scheme.

Hence, any choice of $\vec{d}$ such that

$$\vec{d} - \frac{\vec{\lambda}\Delta t}{2} \; - \; \vec{\nabla}(\vec{\lambda} \cdot \vec{\nabla} u) \tag{6.7}$$

will not alter the second order error term in the approximation, so the corresponding distribution scheme should be second order accurate for the given local data. Therefore, moving the distribution point perpendicular to the local value of $\vec{\nabla}(\vec{\lambda} \cdot \vec{\nabla} u)$ should not change the order of accuracy of the local approximation.

It is important to note here that the second order derivative in (6.7) can be approximated locally by a first order derivative since

$$\vec{\nabla}(\vec{\lambda} \cdot \vec{\nabla} u) \; = \; \vec{\nabla} u_t \tag{6.8}$$

and u_t can be approximated simply from the unlimited high order update using

$$\vec{\nabla} u_t \; = \; \frac{1}{\Delta t}(\vec{\nabla} u^{n+1} - \vec{\nabla} u^n) \; . \tag{6.9}$$

This avoids calculating the second order spatial derivative that appears in (6.7) directly and the overall algorithm remains compact since it still involves only local operations.

6.3 The Monotonicity Region

One of the stages of the FCT algorithm of Section 5 involves constructing bounds on the antidiffusive element contributions to the cell vertices. In (5.8) the bound for a cell is taken to be the most restrictive of those at its three vertices. However, in the context of fluctuation distribution schemes this is not necessary and separate bounds can be considered at each vertex. Thus, in the notation of (5.8),

$$C_T^k \; = \; \min_{\text{vertices}} \begin{cases} R_i^+ & \text{if AEC} > 0 \\ R_i^- & \text{if AEC} < 0 \; , \end{cases} \tag{6.10}$$

where node i corresponds to vertex k of triangle T. These bounds can be used to construct a monotonicity region within each triangle, an example of which is shown in Figure 6.2.

By considering a general FCT-type algorithm, in which the monotonic scheme is written in terms of low order (LO) and high order (HO) updates, the distribu-

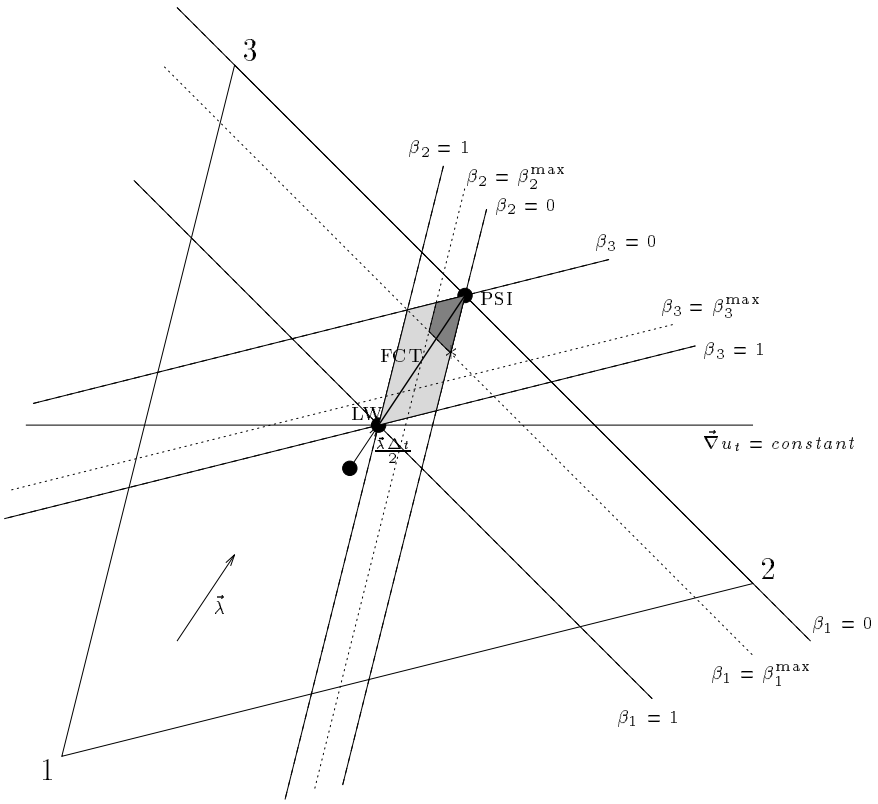

Figure 6.2: A monotonicity region for the distribution point based on the PSI and Lax-Wendroff schemes.

tion coefficients can be expressed as

$$\begin{aligned} \alpha_1 &= \alpha_1^{\mathrm{LO}} + \beta_1 \left(\alpha_1^{\mathrm{HO}} - \alpha_1^{\mathrm{LO}} \right) , \\ \alpha_2 &= \alpha_2^{\mathrm{LO}} + \beta_2 \left(\alpha_2^{\mathrm{HO}} - \alpha_2^{\mathrm{LO}} \right) , \\ \alpha_3 &= \alpha_3^{\mathrm{LO}} + \beta_3 \left(\alpha_3^{\mathrm{HO}} - \alpha_3^{\mathrm{LO}} \right) , \end{aligned} \tag{6.11}$$

in which the β_k are limiting coefficients. In the situation considered here, $\beta_k = 0$ leads to the PSI coefficients while $\beta_k = 1$ returns the Lax-Wendroff scheme. For simplicity, the limiting coefficients will be required to satisfy $0 \leq \beta_k \leq 1$ until otherwise specified. These bounds are illustrated by dashed lines in Figure 6.2. The grey-shaded area in the diagram highlights the region of the triangle within which placing the distribution point will satisfy these bounds.

Conservation requires that

$$\alpha_1 + \alpha_2 + \alpha_3 \; = \; 1 \; , \tag{6.12}$$

so

$$\beta_1 \left(\alpha_1^{\mathrm{HO}} - \alpha_1^{\mathrm{LO}} \right) + \beta_2 \left(\alpha_2^{\mathrm{HO}} - \alpha_2^{\mathrm{LO}} \right) + \beta_3 \left(\alpha_3^{\mathrm{HO}} - \alpha_3^{\mathrm{LO}} \right) \; = \; 0 \; . \tag{6.13}$$

The three terms on the left hand side of (6.13) represent, depending on one's point of view, either the displacement of the distribution point from that of the PSI scheme (in terms of area coordinates) or the additional contributions from the fluctuation to the corresponding vertices of the cell.

The bounds constructed in (6.10) can easily be translated into restrictions on the limiting coefficients since $\beta_k^{\max} = C_T^k$. In general

$$(0 \; =) \beta_k^{\min} \; \leq \; \beta_k \; \leq \; \beta_k^{\max} \; , \quad k = 1, 2, 3, \tag{6.14}$$

which describes three pairs of 'tramlines' parallel to the edges of the triangle, the dotted lines in Figure 6.2. The region for which these bounds are satisfied surrounds the PSI distribution point and is shaded dark grey in the figure. Placing the distribution point anywhere within this shaded area, the monotonicity region, ensures that the subsequent nodal updates will not create any new local extrema at the next time level and as a result imposes stability on the scheme.

Note that the perpendicular distance of each tramline from its parallel cell edge depends linearly on the corresponding β and that $\beta = 0$ defines a line

passing through the low order distribution point while $\beta = 1$ corresponds to the parallel line through the high order distribution point. The aforementioned linear dependence implies that FCT, for which

$$\beta_1 \;=\; \beta_2 \;=\; \beta_3 \;=\; \min_{k=1,2,3} \beta_k^{\max}\,, \tag{6.15}$$

will position the distribution point at the intersection of the straight line joining the Lax-Wendroff and PSI distribution points with the boundary of the monotonicity region.

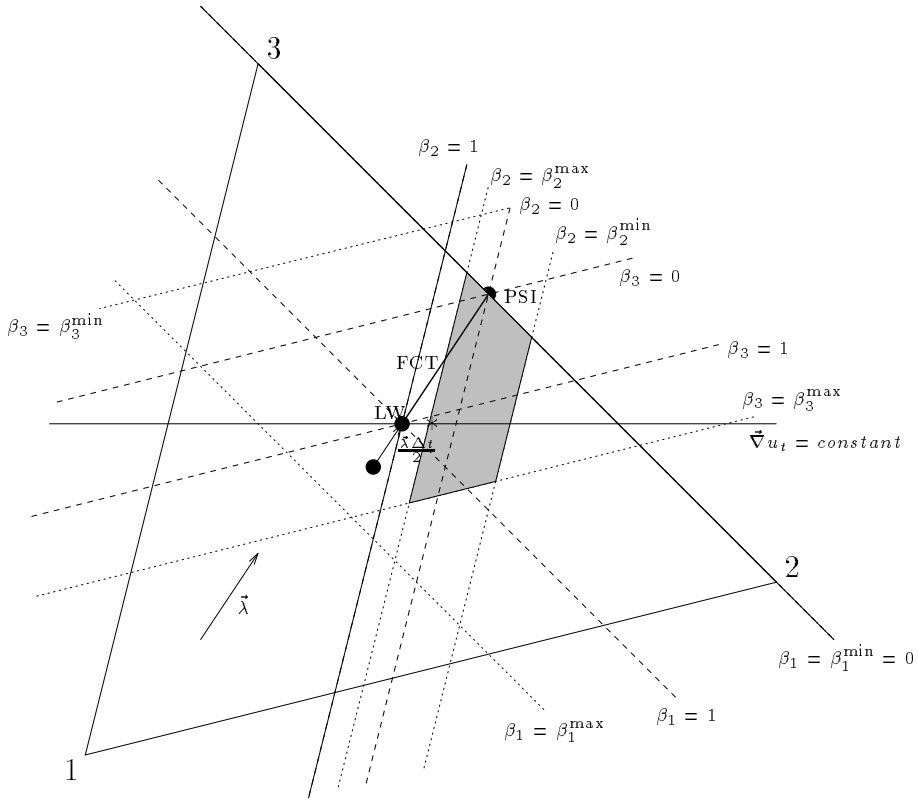

Figure 6.3: An extended monotonicity region for the distribution point based on the PSI and Lax-Wendroff schemes.

The bounds described above may be relaxed to allow $\beta < 0$ or $\beta > 1$, leading to a much larger monotonicity region. For example, restrictions on the antidiffusive element contributions may be constructed as follows:

- Define $P_i^{\pm}$ and $Q_i^{\pm}$ as in (5.6) - although the low order update u_i^{L} could be calculated using the PSI scheme with *maximal* time-step - but now take

nodal limiting factors of

$$(R_i^{\pm})^{\max} = \begin{cases} Q_i^{\pm}/P_i^{\pm} & \text{if } P_i^+ > 0\,,\ P_i^- < 0 \\ 0 & \text{if } P_i^{\pm} = 0\,, \end{cases} \tag{6.16}$$

and

$$(R_i^{\pm})^{\min} = \begin{cases} -Q_i^{\mp}/P_i^{\pm} & \text{if } P_i^+ > 0\,,\ P_i^- < 0 \\ 0 & \text{if } P_i^{\pm} = 0\,. \end{cases} \tag{6.17}$$

- Calculate cell-vertex limiting factors from

$$C_T^k = \begin{cases} (R_i^+)^{\max} & \text{if AEC} > 0 \\ (R_i^-)^{\max} & \text{if AEC} < 0\,, \end{cases}$$

$$C_T^k = \begin{cases} (R_i^+)^{\min} & \text{if AEC} > 0 \\ (R_i^-)^{\min} & \text{if AEC} < 0\,. \end{cases} \tag{6.18}$$

  These are the $\beta_k^{\max}$ of (6.11).

An example of an extended monotonicity region is shown in Figure 6.3. Note that although this increase in flexibility should improve the accuracy of the scheme it may well also allow the limited scheme to be less diffusive than the Lax-Wendroff scheme or let the distribution point move beyond the cell.

6.4 Fluctuation Redistribution

It is clear from the previous sections that it is possible to control the stability and accuracy of a fluctuation distribution scheme by manipulation of the distribution point or, equivalently, redistribution of the fluctuation.

In particular, two schemes have been described, one having second order accuracy (Lax-Wendroff) and the other being monotonic (PSI), which can be combined to produce a scheme with improved properties. In essence this involves constructing the monotonicity region of Section 6.3, then finding the distribution point within this region which minimises the error term according to the equivalent equation (6.6), and redistributing the fluctuation so as to place the distribution point here. When the limiting is applied the distribution point is moved from its high order position towards its low order position along some path which minimises any loss of accuracy until the distribution satisfies the local monotonicity constraints.

The path along which the distribution point travels is dictated by the 'preferred direction' (perpendicular to $\vec{\nabla} u_t$) which is suggested by (6.6). Given that the dominant error term of the scheme is proportional to some approximation to

$$\left(\vec{d} - \frac{\vec{\lambda} \Delta t}{2} \right) \cdot \vec{\nabla} (\vec{\lambda} \cdot \vec{\nabla} u) \, , \tag{6.19}$$

the following algorithm is suggested:

- Use the PSI scheme to construct a low order, monotonic update.
- Construct the monotonicity region surrounding the low order distribution point using the bounds on the cell→vertex contributions defined by either (6.10) or (6.18).
- Calculate the high order updates due to the Lax-Wendroff scheme.
- Find the line passing through the high order distribution point perpendicular to the locally constructed value of $\vec{\nabla} u_t$ (*i.e.* a contour line of u_t).
- Calculate the position of the point in the monotonicity region closest to the line defined above. If the two intersect then take the point of intersection closest to the high order distribution point.
- Find the limiting coefficients β_k which place the distribution point in this position and hence calculate the limited antidiffusive cell→vertex contributions.
- Add the limited antidiffusive contributions to the low order updates.

The limited distribution points are indicated by asterisks in Figures 6.2 and 6.3. Note that when the contour line does not intersect the monotonicity region the limited distribution point will be at a corner of the region.

7 Results

Numerical experiments have been carried out to test the schemes described in this report. The first case presented here is the advection of an initial profile

given by the double sine wave function

$$u \;=\; \sin(2\pi x)\sin(2\pi y)\;, \tag{7.1}$$

with velocity $\vec{\lambda} = (1,1)^T$ over the domain $[0,1] \times [0,1]$. This problem has been solved on three types of grid each of which is illustrated in Figure 7.1. Periodic boundary conditions are applied.

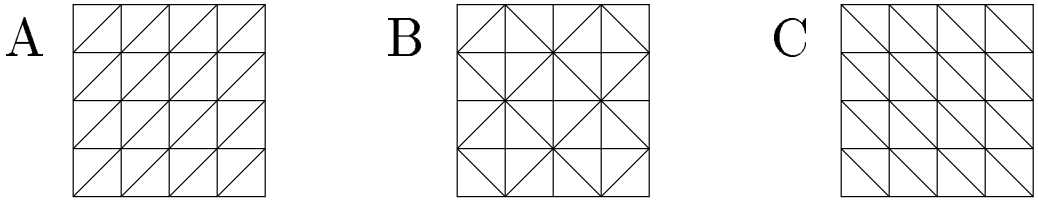

Figure 7.1: The three grid types used for the numerical experiments.

Figure 7.2 shows two solutions to the above problem obtained on a 64×64 type B grid, one obtained using the standard PSI scheme, (2.6) and (2.7), and the second including the area weighting of the nodal updates described in Section 2.3. Not only does the area weighted scheme advect the shape of the initial profile much better but the resulting solution is also slightly smoother. Further evidence of this improvement in accuracy, particularly in the L_∞ norm, is provided in Table 1 which shows the errors in the solution at $t = 1.0$ and compares them with the Lax-Wendroff scheme of (2.12). As expected the last of these is by far the most accurate since it is one order of accuracy higher than the other two.

Scheme	L_1	L_2	L_∞	Peak value
PSI	0.1914	0.2109	0.3707	0.629
Area weighted PSI	0.1849	0.2023	0.2864	0.714
Lax-Wendroff	0.0131	0.0143	0.0215	0.998

Table 1: Error norms of solutions for the double sine wave problem at $t = 1.0$ on a 64×64 type B grid.

The next comparison presented is of all the schemes without the application of any post-processing limiting procedure. A detailed accuracy study has been

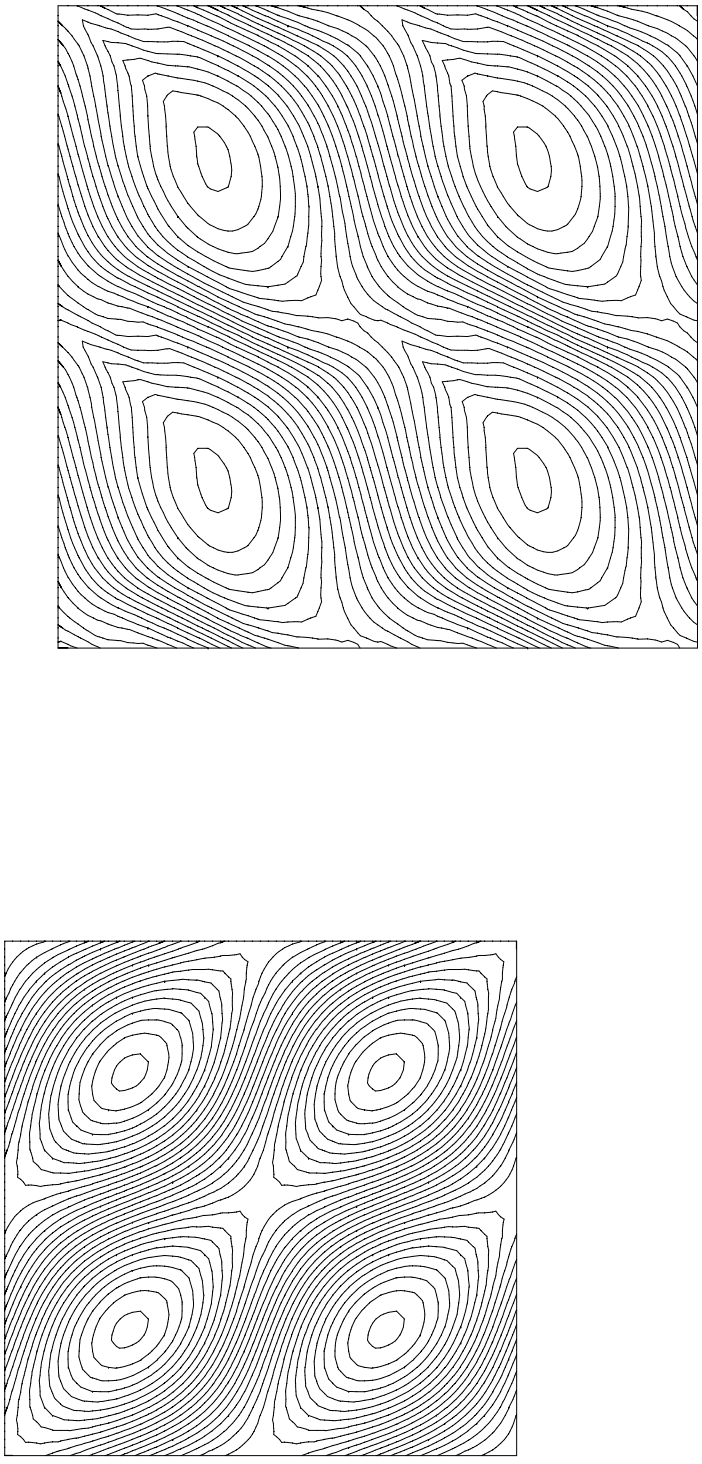

Figure 7.2: Solutions for the double sine wave test case.

carried out for each of the schemes under consideration and the results for the double sine wave test case described above are shown in Figure 7.3. dt/dx takes the value of 0.08 throughout for this test case.

Error estimates in the L_2 norm for the solution when $t = 1$ are shown for five different schemes. The errors in the L_1 and L_∞ norms showed very similar behaviour. The least accurate method is the PSI scheme which can be seen in practice in Table 2 to not even attain first order accuracy on any of the three regular grids shown in Figure 7.1. The Lax-Wendroff scheme consistently achieves second order accuracy on each of the grids and gives similar answers for each case. The predictor-corrector scheme is less reliable. On the type A grid it is comparable to Lax-Wendroff but on grid B the error actually increases as the grid is refined (hence the lack of an entry in the table). The consistent finite element scheme based on PSI and combined with implicit Crank-Nicolson time-stepping does indeed exhibit third order accuracy on grid A, but reduces to less than second order on the other two types of grid. In fact, on grid C it ceased to be the most accurate of the schemes considered. For comparison, the results are pictured in Figure 7.3 alongside those of a cell-centre upwind finite volume scheme which combines a linear reconstruction algorithm with the MLG limiter [2]. The Lax-Wendroff scheme is significantly more accurate on all but grid A and even here it achieves a higher order of accuracy, although it should be noted that the cell-centre scheme includes a limiter which makes it monotonic.

Scheme	Grid A	Grid B	Grid C
PSI	0.66	0.75	0.81
Lax-Wendroff	2.01	2.01	2.01
Predictor-corrector	2.01	-	1.61
Consistent PSI	2.96	1.84	1.84
Cell-centre FV	1.84	0.92	1.52

Table 2: L_2 orders of accuracy of the unlimited schemes on the three grid types calculated when $dx = 1/128$.

The improvement in accuracy is illustrated even more dramatically by a second

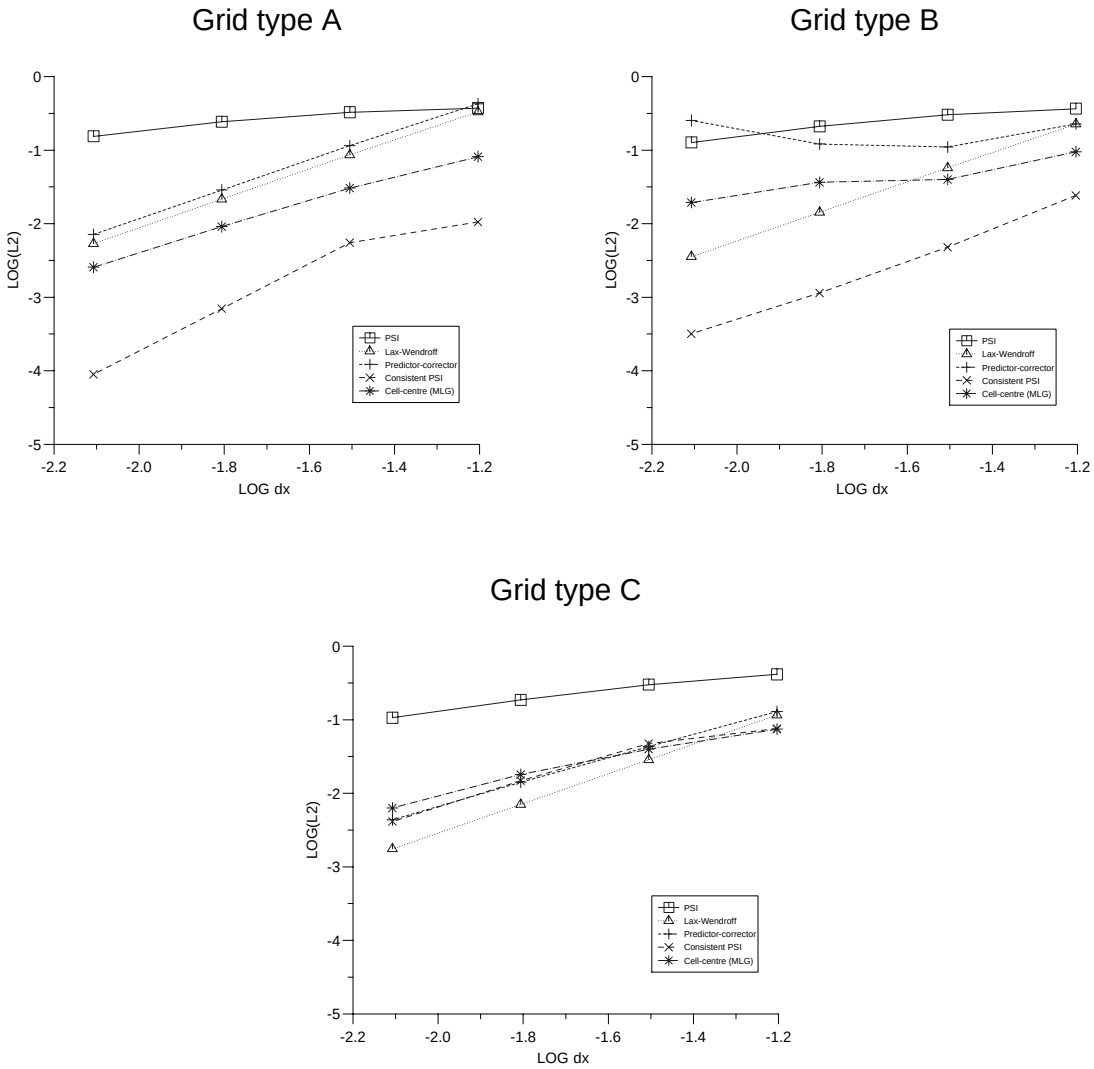

Figure 7.3: L_2 errors for the double sine wave test case on the three different types of grid.

test case. It involves the circular advection of the 'cone' given by the initial conditions

$$u = \begin{cases} \cos^2(2\pi r) & \text{for } r \leq 0.25 \\ 0 & \text{otherwise} \end{cases} \tag{7.2}$$

where $r^2 = (x + 0.5)^2 + y^2$, with velocity $\vec{\lambda} = (-2\pi y, 2\pi x)^T$ around the domain $[-1, 1] \times [-1, 1]$, the solution being continually set to zero at each of the inflow boundaries. The initial profile should be advected in a circle without change of shape until it returns to its original position when $t = 1.0$.

In the numerical experiments the ratio $dt/dx = 0.04$. Three solution profiles obtained on a 64×64 type B grid are shown in Figures 7.4 and 7.5 using the schemes *without* limiters being applied. After one revolution the PSI scheme has reduced the height of the peak from 1.0 to 0.32 and is extremely diffusive, particularly in the streamwise direction. The Lax-Wendroff scheme keeps the height of the peak at 0.82 but oscillations are obvious in the wake of the cone so that some form of limiting procedure is clearly necessary. Less clear is a small phase lag which positions the peak slightly downstream of its correct position. Qualitatively, the predictor-corrector scheme gives very similar results, a small phase lag with downstream oscillations. From now on only the Lax-Wendroff scheme will be considered since it is far more reliable (as indicated in Table 2), usually more accurate and computationally less expensive. When the consistent mass matrix and Crank-Nicolson time-stepping are introduced for the PSI scheme small oscillations can be seen in front of the profile, although the cone is now at 94% of its original height - the best of the solutions shown. It should be noted though that the nature of the test case, in which the advection velocity changes through a full 360° significantly reduces the size of the oscillations in this last case.

The same test case is illustrated on the same grid in Figures 7.6, this time for schemes which have had monotonicity conditions imposed on them via the application of limiters. The oscillations have now disappeared from both the Lax-Wendroff scheme (combined with the fluctuation redistribution technique described in Section 6) and the consistent PSI scheme (with FCT) although the peak values of the solution have been reduced to 0.76 and 0.87 respectively. They

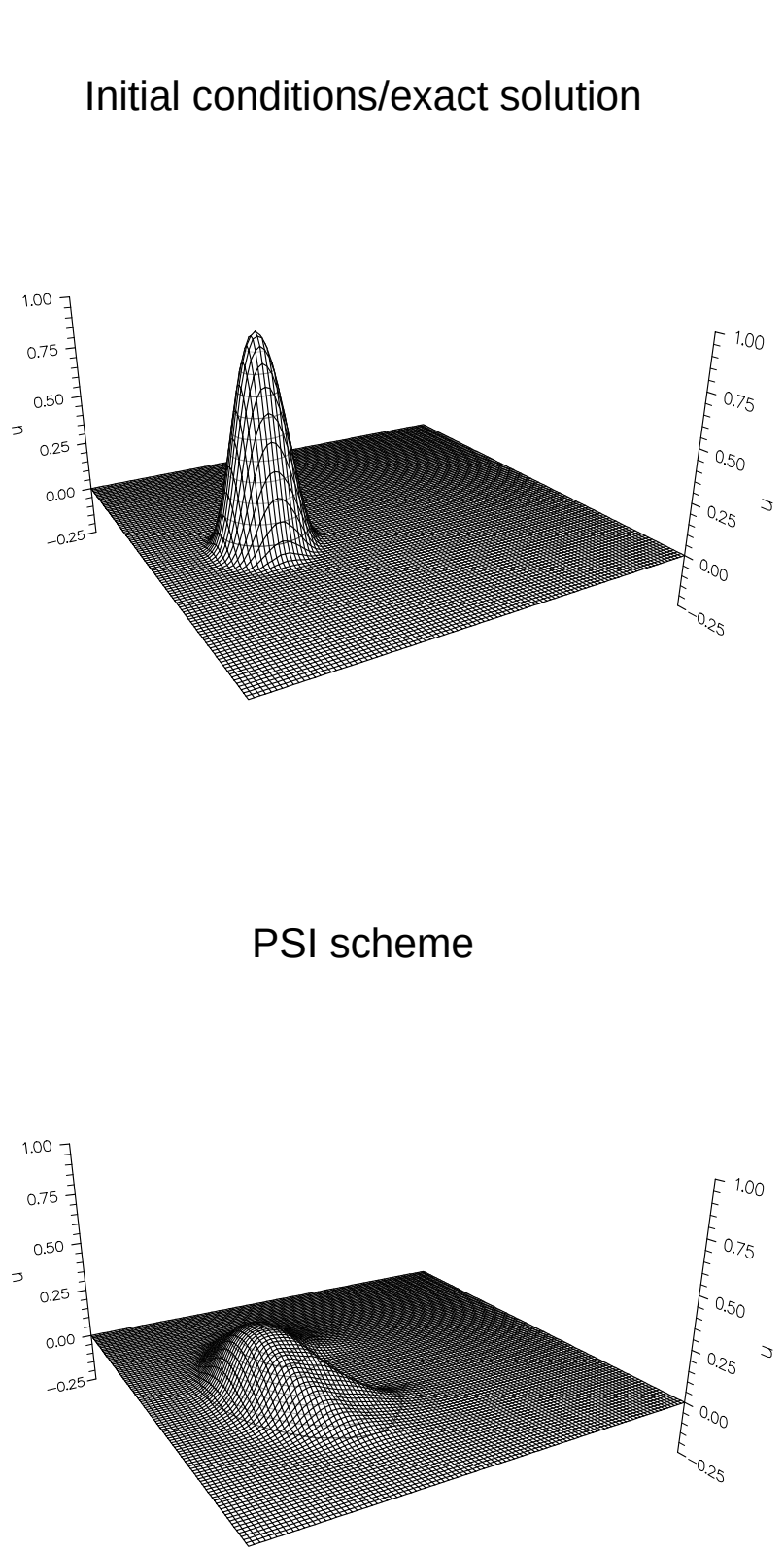

Figure 7.4: Solutions for the rotating cone test case.

Lax-Wendroff scheme

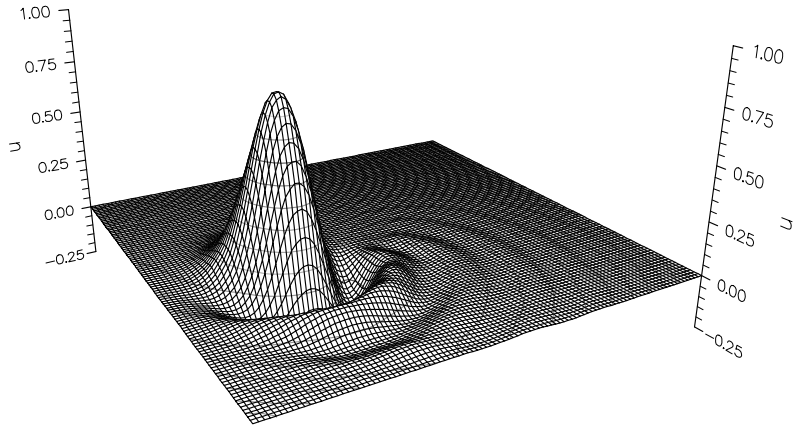

Consistent PSI scheme

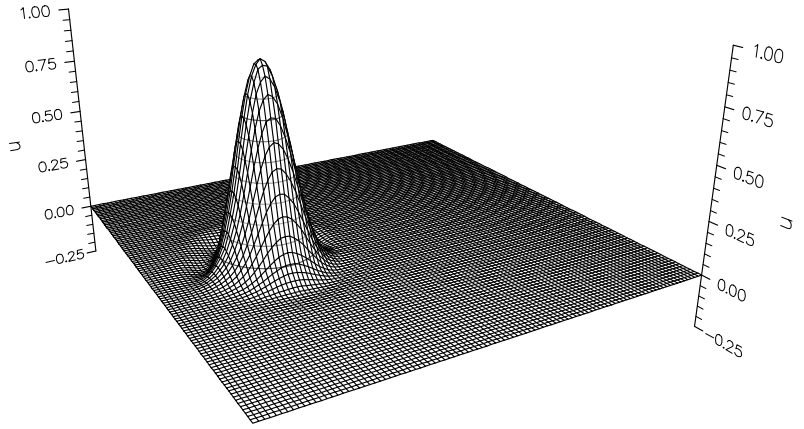

Figure 7.5: Solutions for the rotating cone test case.

are compared with the cell-centre upwind MLG scheme [2], Figure 7.7, which is also monotonic but the peak value here is only 0.62 after one revolution. It should be noted, though, that the cell-centre scheme performs considerably better on grids of type A or C and is then comparable with the limited Lax-Wendroff scheme.

The practical order of accuracy of the monotonic schemes can be investigated using the double sine wave test case. Table 3 shows error estimates which are typical of the test case. The monotonicity constraint has little effect on the error approximations in the L_1 and L_2 norms but the fluctuation redistribution technique is significantly better than a standard FCT approach when the L_∞ norm is considered although some loss of accuracy is still incurred.

Scheme	L_1	L_2	L_∞	Peak value
Lax-Wendroff	0.0131	0.0143	0.0215	0.998
Lax-Wendroff + FCT	0.0132	0.0144	0.0263	0.996
Lax-Wendroff + FR	0.0129	0.0143	0.0230	0.998
Consistent PSI	0.0009	0.0011	0.0041	0.999
Consistent PSI + FCT	0.0010	0.0015	0.0124	0.994

Table 3: Error norms of solutions to the double sine wave problem at $t = 1.0$ on a 64×64 type B grid.

The effectiveness of the new method is also illustrated in Figure 7.8, particularly on the finer grids. The fluctuation redistribution scheme remains close to the unlimited Lax-Wendroff scheme on each of the grids while the FCT solution deteriorates on the finer grids for both the Lax-Wendroff and consistent PSI schemes. It is interesting to note that the numerical order of accuracy in the L_∞ norm on the finest grid is 2.0 for the Lax-Wendroff scheme with or without fluctuation redistribution, but reduces to 1.28 when FCT is used, while FCT reduces the order of accuracy of the consistent PSI scheme from 1.57 to 0.97. In the L_1 and L_2 norms little difference is detected in the error from that of the non-monotonic scheme on any of the grids, although typically fluctuation redistribution is more accurate than FCT on the finer grids.

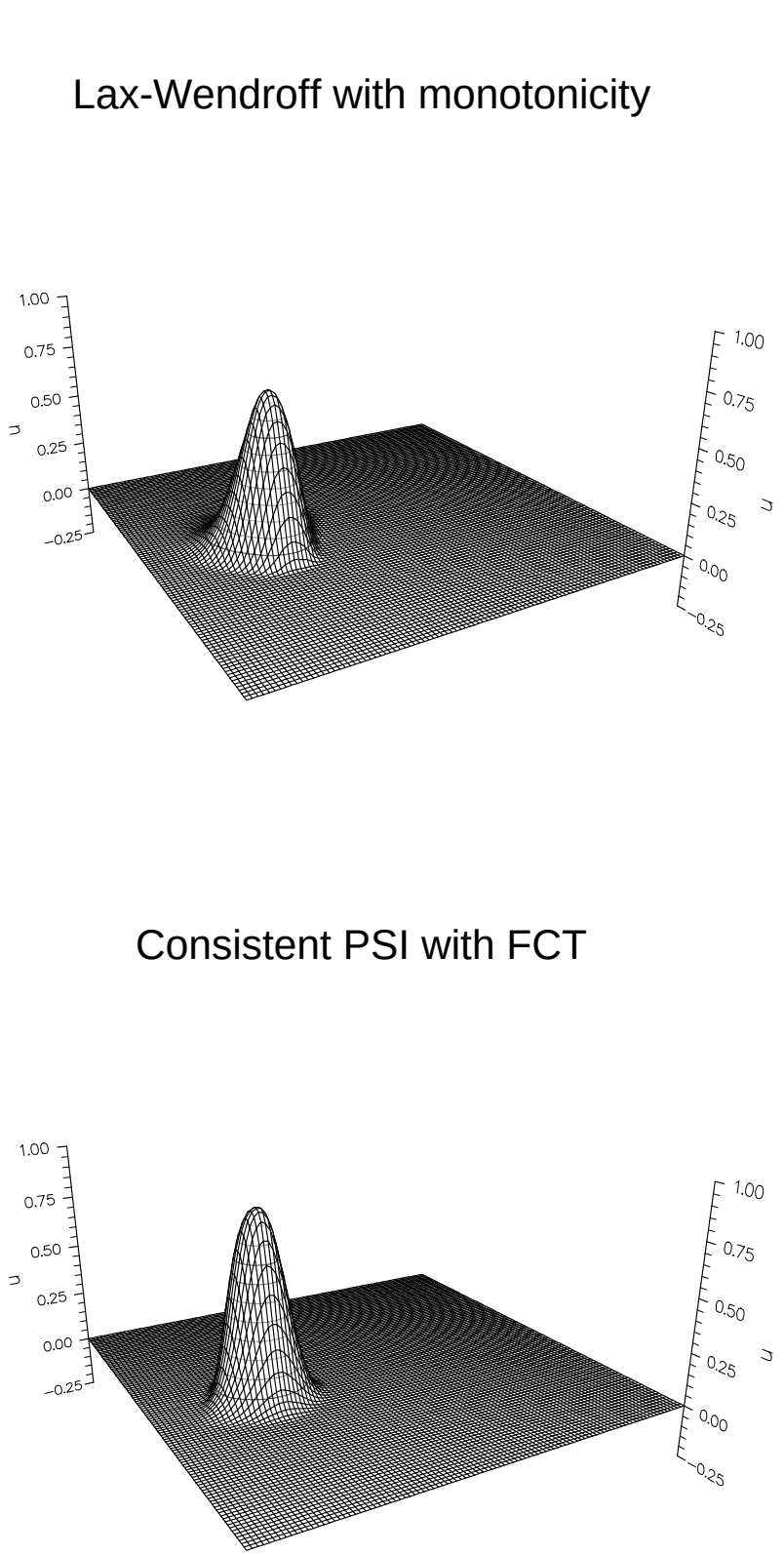

Figure 7.6: Monotonic solutions for the rotating cone test case.

Figure 7.7: Monotonic solutions for the rotating cone test case.

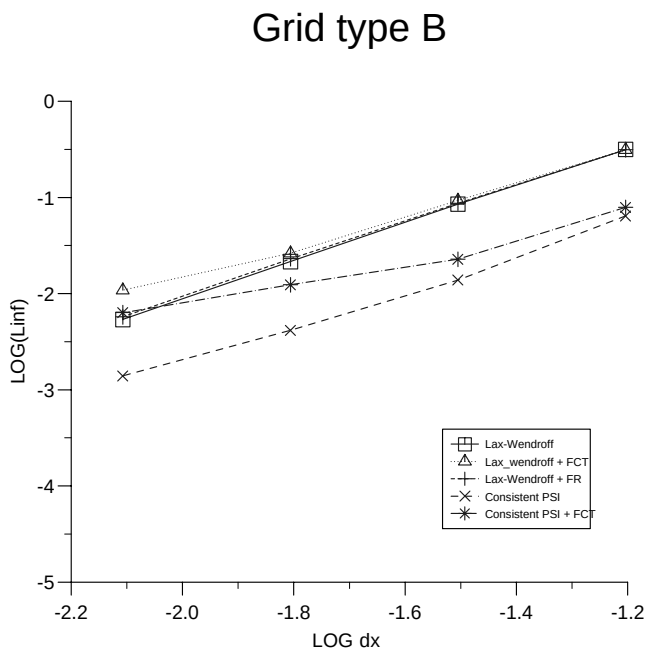

Figure 7.8: L_∞ errors for the double sine wave test case.

Finally, the schemes have also been compared on distorted grids. The grid shown in Figure 7.9 is a random perturbation of a 64×64 type B grid in which each interior node has been moved by a distance of at most $dx/2$ in both coordinate directions. As expected, the accuracy deteriorates with the irregularity of the grid. Table 4 should be compared with Table 3 to see the loss in accuracy, which is considerably worse in the case of FCT particularly in the L_∞ norm. Typically, on the finest perturbed grids, the order of accuracy is no worse than 1.8 for the fluctuation redistribution algorithm, which matches the order of the unlimited Lax-Wendroff scheme, while applying the FCT algorithm gives considerably worse results.

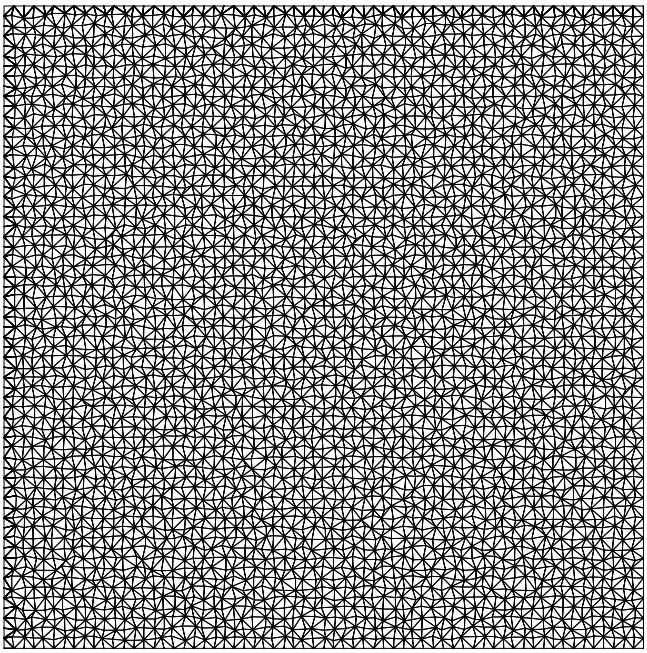

Figure 7.9: The perturbed 64×64 grid.

Scheme	L_1	L_2	L_∞	Peak value
Lax-Wendroff	0.0149	0.0165	0.0359	1.001
Lax-Wendroff + FCT	0.0161	0.0188	0.1045	0.975
Lax-Wendroff + FR	0.0151	0.0172	0.0847	0.985

Table 4: Error norms of solutions to the double sine wave problem at $t = 1.0$ on a 64×64 type B grid.

8 Conclusions

In this report the problem of achieving high order accurate numerical solutions to the two-dimensional scalar advection equation using upwind fluctuation distribution schemes on triangular grids has been addressed.

Three approaches have been compared: a finite element method [6], a predictor-corrector algorithm and the Lax-Wendroff scheme [3]. The consistent finite element scheme has been shown to achieve third order accuracy on some regular grids but it involves the inversion of a mass matrix. The predictor-corrector scheme is much faster but not particularly robust whereas the single step Lax-Wendroff distribution scheme is second order accurate on all of the grids considered. It is usually more accurate than the predictor-corrector scheme (they are equivalent in some situations) and on some regular grids it even improves on the consistent finite element scheme.

Each of the above approaches is not inherently monotonic. However, this property may be imposed using an FCT approach as described in this report. In the case of the Lax-Wendroff scheme, though, a more sophisticated approach has been devised which involves a redistribution of the fluctuation. Bounds on the contributions to each node are calculated in a similar manner to those used in FCT and the distribution coefficients are then altered so that these bounds are satisfied. A study of the equivalent equation of the scheme reveals that there is also a preferred direction for the movement of the distribution point - the point which geometrically represents the local distribution - which should improve the retention of second order accuracy even when the limiting is applied. Flux-corrected transport is a special case of fluctuation redistribution.

In practice, the Lax-Wendroff scheme with the additional fluctuation redistribution step has proved to be second order accurate in each case tested here. This is not true of FCT for which the L_∞ error deteriorates rapidly as the grid is refined. The result is a fast, accurate and robust fluctuation distribution scheme based on multidimensional upwind techniques for the solution of the scalar advection equation. Furthermore, it should be straightforward to extend these schemes to nonlinear systems of equations in the same manner as in the steady state case

[8], although it remains to completely overcome the lack of robustness of these extensions near to stagnation points.

Acknowledgements

The authors would like to thank Prof. M. J. Baines for his contributions to this work, Dr Nick Birkett for supplying the subroutines for the GMRES algorithm and the EPSRC for providing the funding for the first author.

References

[1] T.J.Barth, private communication.

[2] P.Batten, C.Lambert and D.M.Causon, 'Positively conservative high-resolution convection schemes for unstructured elements', *Int. J. for Numerical Methods in Engineering*, **39**:1821–1838, 1996.

[3] H.Deconinck, R.Struijs, G.Bourgois and P.L.Roe, 'High resolution shock capturing cell vertex advection schemes for unstructured grids', *Computational Fluid Dynamics*, number 1994–05 in VKI Lecture Series, 1994.

[4] C.Hirsch, Numerical Computation of Internal and External Flows, volume 1, Wiley, 1990.

[5] R.Löhner, K.Morgan, M.Vahdati, J.P.Boris and D.L.Book, 'FEM-FCT: combining unstructured grids with high resolution', *Communications in Applied Numerical Methods*, **4**:717–729, 1988.

[6] J.März, 'Improving time accuracy for residual distribution schemes', Project Report 1996–17, von Karman Institute for Fluid Dynamics, 1996.

[7] R.W.MacCormack, 'The effect of viscosity in hypervelocity impact cratering', AIAA Paper 69-354, 1969.

[8] H.Paillère, E.van der Weide and H.Deconinck, 'Multidimensional upwind methods for inviscid and viscous compressible flows', *Computational Fluid Dynamics*, number 1995–12 in VKI Lecture Series, 1995.

[9] P.L.Roe, 'Geometry of fluctuation-splitting schemes', unpublished.

[10] Y.Saad, 'Krylov subspace techniques, conjugate gradients, preconditioning and sparse matrix solvers', *Computational Fluid Dynamics*, number 1994–05 in VKI Lecture Series, 1994.

[11] Y.Saad and M.Schultz, 'GMRES: a generalised minimum residual algorithm for resolving nonsymmetric linear systems', *SIAM J. Scientific and Stat. Comp.*, **7**:856–869, 1986.

[12] S.T.Zalesak, 'Fully multidimensional flux-corrected transport algorithms for fluids', *J. Comput. Phys.*, **31**:335–362, 1979.